Available online at www.sciencedirect.com
SCIENCE DIRECT
Diamond & Related Materials 15 (2006) 71 – 79
DIAMOND AND RELATED MATERIALS
www.elsevier.com/locate/diamond

Surface and optical analysis of SiC_x films prepared by RF-RMS technique

A. Mahmood [a], S. Muhl [b], R. Machorro [c,*], A. Lousa [d], J. Esteve [d], J. Heiras [c]

[a] *Applied Physics Division, PINSTECH, P.O. Nilore, Islamabad, Pakistan*
[b] *Instituto de Investigaciones en Materiales, UNAM, Apdo. Postal 670-360, D.F., 045110, México*
[c] *Centro de Ciencias de la Materia Condensada-UNAM, Apdo. Postal 2681, Ensenada, B.C., 22800, México*
[d] *Departament de Física Aplicada i Òptica, Universitat de Barcelona, Avda. Diagonal 647, E-08028 Barcelona, Catalunya, Spain*

Received 23 September 2004; accepted 6 July 2005
Available online 15 August 2005

Abstract

Silicon Carbide thin films have been prepared by RF reactive magnetron sputtering of a silicon target in a mixture of Ar and CH_4. Surface analysis was performed by X-ray photoelectron spectroscopy (XPS) to examine the elemental bonding at the surface and in bulk of the material. Optical analysis was carried out by ellipsometry to study the optical constants (n and k) and band gap of the films. Transmission and scanning electron microscopy, FTIR and X-ray diffraction, were employed to supplement our results. The near surface of SiC exposed to atmosphere was primarily composed of SiO_2 along with amorphous carbon while the bulk of the material was SiC. At higher plasma power and lower CH_4 concentration, the graphitic phase in the surface decreases and the refractive index increases while surface oxide layer remains present.

Keywords: Silicon carbide; Thin films; XPS; Ellipsometry; Surface analysis; Optical properties

1. Introduction

Silicon carbide, SiC_x is an important material for the semiconductor industry both in crystalline [1,2] as well as in amorphous form [3,4]. Crystalline silicon carbide is a large band gap semiconductor (>2 eV) with high thermal stability (melting point ~ 2800 °C), good mechanical properties, large thermal conductivity (~3.9 W/cm per °C), high electric break down field ($\sim 4 \times 10^6$ V/cm) and a saturation drift velocity of approximately 2×10^7 cm/s [5,6]. Such properties make crystalline SiC a very attractive candidate for high temperature and high power applications in the electronic industry [7,8]. Amorphous silicon carbide (a-$Si_{1-x}C_x$) is a wide band gap semiconductor and is potentially useful for a variety of applications including solar selective coatings.

Unfortunately, the high melting point and the diversity of crystal structures adopted by SiC make difficult to prepare good quality single crystal or polycrystalline samples. SiC thin films have been prepared by high temperature chemical vapour deposition but this technique produces unintentionally doped films with high concentration of lattice defects. Several methods involving lower temperature processing, such as thermal and laser recrystallization [9,10], plasma and hot-filament enhanced chemical vapor deposition [11,12], low pressure chemical vapor deposition [13], gas source molecular beam epitaxy [14] and UHV reactive DC magnetron sputtering [15,16], have been attempted to overcome these difficulties. However, the present knowledge concerning the relation between physical properties and preparation processes of different forms of silicon carbide is very limited. The purpose of this work is the study of the surface oxygen content in SiC thin films prepared by RF reactive magnetron sputtering (RF-RMS) in order to establish the dependence of optical properties on chemical composition and structure on deposition parameters. Our results suggest that SiC is a wide band gap semiconductor whose native oxide is suitable to be used as a MOS insulator in electronic devices.

* Corresponding author.
E-mail address: roberto@ccmc.unam.mx (R. Machorro).

0925-9635/$ - see front matter © 2005 Elsevier B.V. All rights reserved
doi:10.1016/j.diamond.2005.07.006

2. Experimental Procedure

A turbomolecular pumped stainless steel UHV vacuum system with a base pressure lower than 1.3×10^{-7} Pa was used for film preparation. The deposition chamber is equipped with a 4-inch diameter magnetron source and stainless steel substrate stage/heater. Fine wire thermocouples are used to correlate the temperature of the surface of the P-etched silicon substrates to the temperature of the substrate holder. Sputtering was performed using different argon and methane gas mixtures, Ar/CH_4 of 80:20, 70:30, 50:50 and 40:60 (purity of gases was 99.999%), at RF plasma powers of 100 and 200 W and a gas pressure of 0.4 Pa. The gas pressure and flows were measured using a MKS capacitance manometer and mass flow controllers. The chamber gas pressure was controlled by manually adjusting the position of the gate valve between the chamber and the turbomolecular pump. The substrate to target distance was maintained at 5 cm in all experiments.

The following preparation procedure was used to clean the target and to carbonize the surface of the substrates. After the required substrate temperature was attained, 0.08 Pa of CH_4 was introduced for 10 min, the chamber pressure was then increased to 0.4 Pa through the addition of the argon and the plasma was ignited with a shutter covering the substrate. The shutter was then removed to deposit the film during a given time, constant for all samples. After growth the substrates were moved to the load lock chamber using the substrate manipulator, and only when the substrate temperature was less than 100 °C, the gas flow was turned off and the substrate removed from the system. Pieces of silicon, one mm wide, were used to mask part of the substrate to facilitate the film thickness measurement using the Dektak IIA profilometer. The samples were analyzed using a Nicolet 510P FTIR spectrophotometer, and a Siemens D500 X-ray powder diffractometer using CuKα radiation. For the XPS analysis, a Riber system equipped with a Cameca-Mac3 electron energy analyser was employed using the K_α line of Mg (1253.6 eV) as excitation source. The spectra were collected acquiring data every 0.2 eV with an energy resolution of 0.8 eV. The binding energy of each peak was calibrated by using the 1 s core level of carbon at 284.5 eV as a reference.

The complex refractive index, as a function of photon energy, provides a number of physical characteristics of the material: band gap, light absorption or transparency, its colour, etc. Furthermore, a convenient way to measure the refractive index and thickness of thin solid films is by ellipsometry since it is a non-intrusive sensitive technique. For this optical analysis a UVISEL Jobin Yvon ellipsometer was employed.

The ellipsometer measures the amplitude and phase change of the perpendicular *component s* relative to the parallel *component p* of monochromatic polarized light reflected from a surface, after a known light beam is reflected from the surface under study [8]. The measurable parameters (Ψ, Δ) are related to the film and substrate properties by means of the complex reflectance ratio:

$$\rho = \frac{r_p}{r_s} \tan\psi \cdot \exp(i\Delta), \tag{1}$$

where, r_p and r_s are the Fresnel reflection coefficients for light polarized parallel and perpendicular to the plane of incidence. An analytical solution to the equation is not an easy task, except for simple cases. A curve fitting procedure between the measured data and a proposed model is required to obtain the film properties. Initially, in our study we assumed a homogeneous film with well-defined interfaces. The refractive index wavelength (or photon energy) dependency was simulated using a double Lorentz oscillator model:

$$\varepsilon(\omega) = \varepsilon_\infty + \sum_{j=1}^{2} \frac{f_j \omega_{0j}^2}{\omega_{0j}^2 - \omega^2 + i\gamma_j \omega}, \tag{2}$$

where ε_α is the high frequency dielectric constant, f_j is the oscillator strength, ω_{0j} is the oscillator frequency and γ_j is the damping factor. The refractive index is obtained from the expression $\varepsilon = n^2$.

The ion beam (IBA) facilities at the University of Mexico [17] based on a vertical single ended 5.5-MV Van de Graff accelerator was used to obtain the surface density (atoms/cm^2) and the composition of the SiC_x films. A low energy $^2H^+$ beam instead of the $^4He^+$ RBS standard technique was chosen to analyze the samples because the carbon real density can be obtained from both the $^{12}C(d,p)^{13}C$ nuclear reaction (NR) peak and the $^2H^+$ elastically backscattered part of the spectrum. A 1140-keV deuterium beam incident perpendicular to the sample with a laboratory detector angle of $\theta_{lab} = 165°$ was used. At this energy the Coulomb barrier for the Si nuclei is high and the elastic cross-section is approximately three orders of magnitude larger than the possible $^{28}Si(d,p)$ and $^{28}Si(d,\alpha)$ nuclear reactions and therefore their contribution to the particle spectrum is negligible. A 300-μm surface barrier detector with standard electronics was used to measure the energy of the emitted particles. The particle energy spectra collected from the samples were analyzed using the SIMNRA program [18]. This computer code is more versatile than the more often used RUMP program [19], because it includes NR cross-sections, non-Rutherford cross-sections, and multiple and plural scattering.

3. Results

From 2-θ X-ray diffraction measurements it is observed that the majority of the films were amorphous. Only films prepared using the conditions of 100 W, Ar/CH_4 60:40, 800 °C showed indications of diffraction peaks related to silicon carbide.

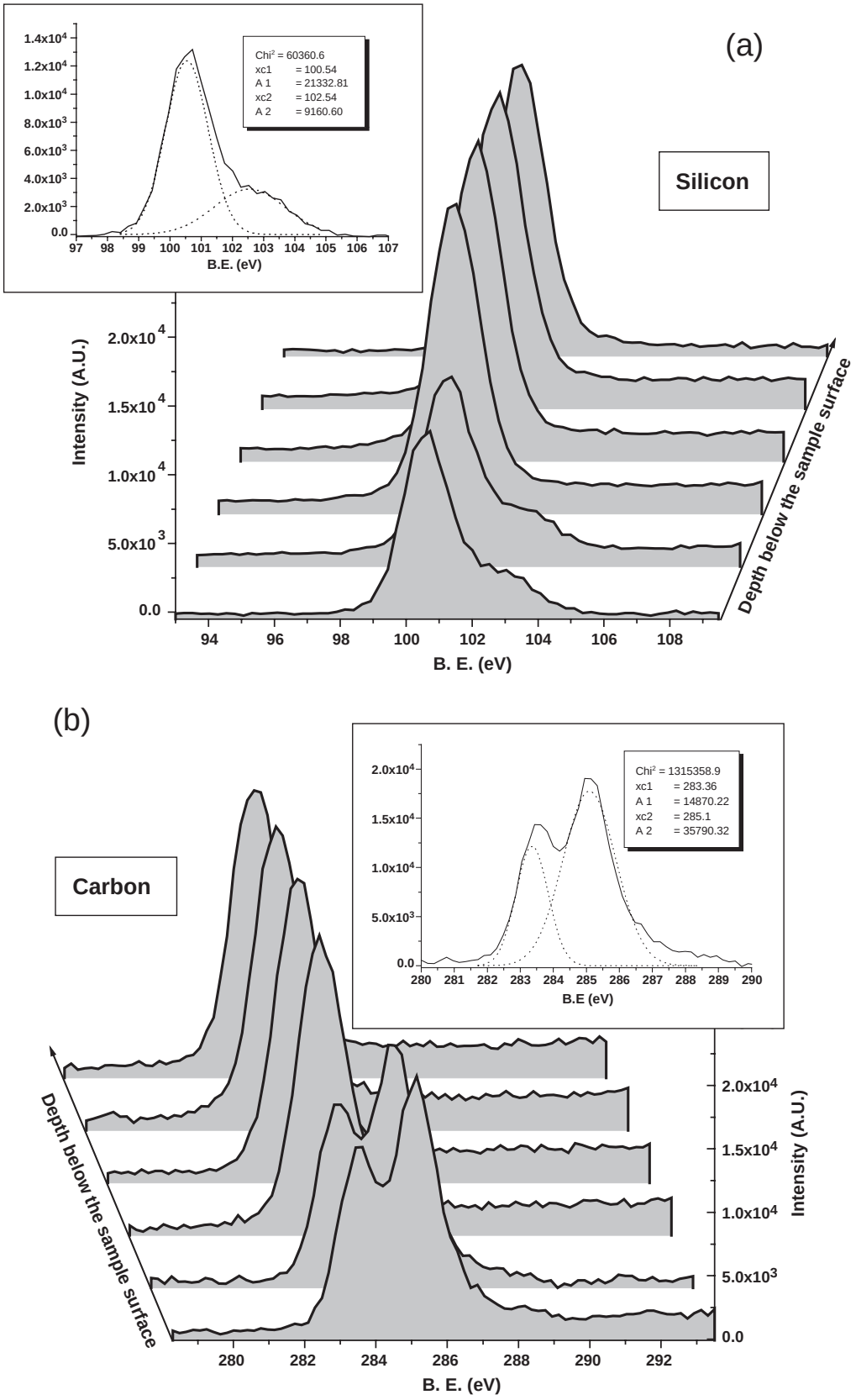

Fig. 1. XPS spectra for (a) Si2p (b) C1s (c) Ar2p (d) O1s taken every 0.2 eV with a resolution of 0.8 eV (calibration reference: 1s core level of carbon at 284.5 eV). The first front spectra shown are of the surface of the sample and the others were taken progressively following erosion steps of approximately 50 nm. (Window) The inserts show the details of the Lorentzian simulation of the relevant double peaks.

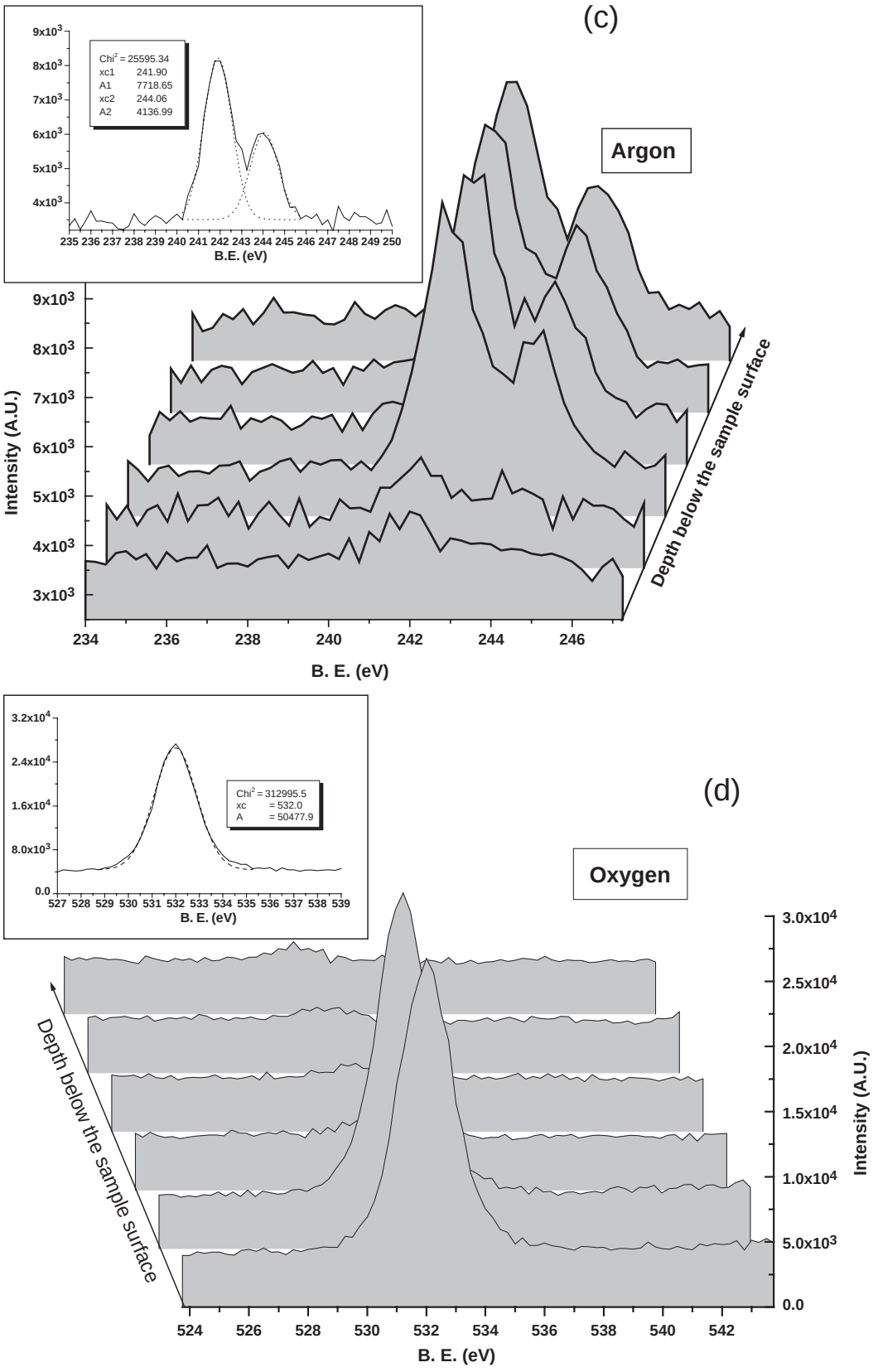

Fig. 1 (*continued*).

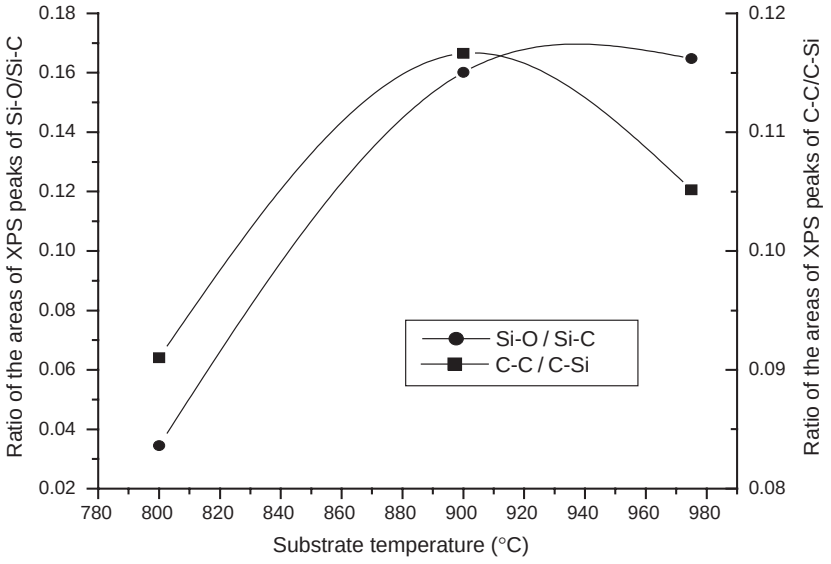

Fig. 2. The variation of Si–O/Si–C and C–C/C–Si ratios as a function of the substrate temperature.

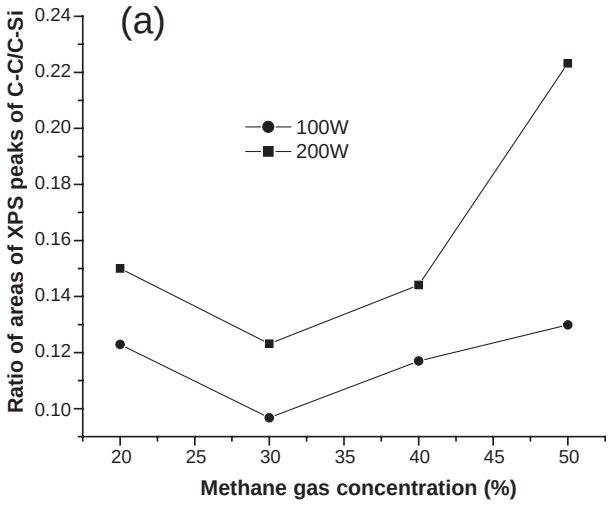

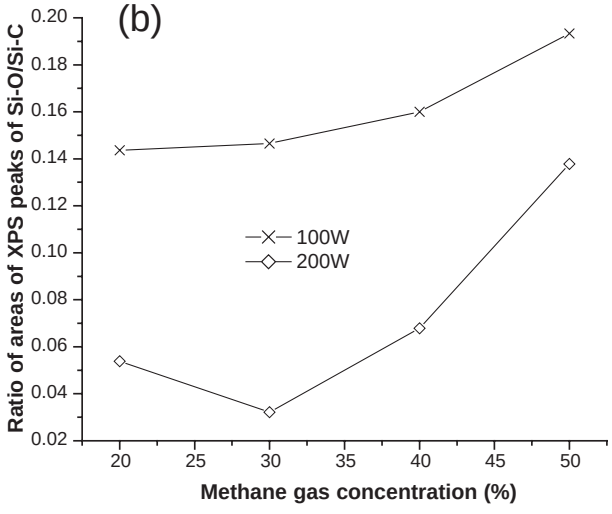

Fig. 3. The variation of the (a) Si–O/Si–C and (b) C–C/C–Si ratios with the percentage of CH_4 in the gas for plasma powers of 100 and 200 W.

Fig. 1a, b, c and d show the XPS spectra for Si2p, C1s, Ar2p and O1s, respectively. The first front spectra shown are of the surface of the sample and the others were taken progressively following erosion steps of approximately 50 nm. The inserts show the details of the Lorentzian simulation of the relevant double peaks. The silicon peaks are seen to be centred at 100.54 and 102.54 eV and correspond to silicon bonded to carbon and oxygen [20,21]. No XPS peak associated with Si–H bonds were found [22], and the silicon oxide bonds are detected only in the surface of the sample. The carbon peaks are centred at 283.36 and 285.10 eV and correspond to carbon bonded to silicon and carbon [23,24]. The carbon–carbon bonds are found mainly in the surface layers, and no XPS peak associated with C–H bonds were observed [25]. The argon data shows that it is present throughout the film but with a much lower

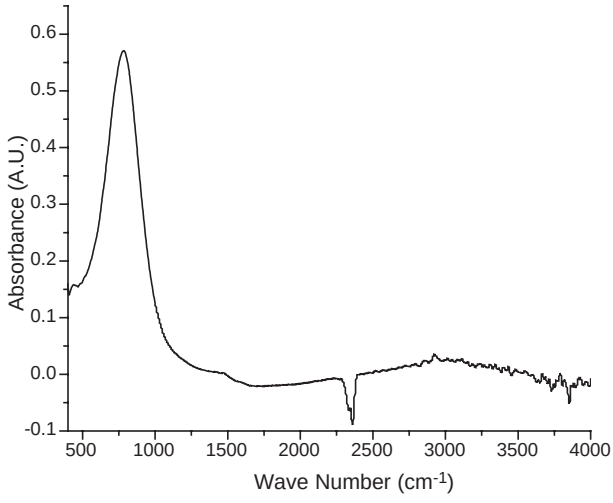

Fig. 4. A typical FTIR spectra of the film prepared using a plasma power of 200 W, $Ar/CH_4 = 70/30$ and substrate temperature of 850 °C.

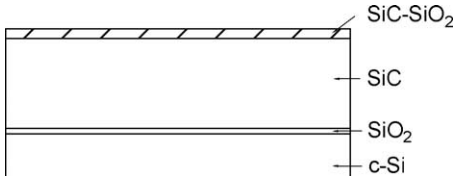

Fig. 5. Stack model used to fit ellipsometric parameters: SiO_2 24 Å thick, SiC+ voids from 2000 to 7000 Å thick, SiO_2+SiC from 60 to 130 Å thick with a concentration of SiO_2/SiC of 30% to 80%.

concentration in the sample surface layers. In the bulk of the sample, the Ar signal can be seen as a double peak centred at 241.90 and 244.06 eV. This type of signal is normally associated with two chemical bonding configurations for the detected element. Obviously, this is not the case for Ar in the SiC_x deposits, but the signal may indicate that the argon is trapped in voids within the film and the doublet appears because of Van der Waals bonding between the Ar atoms. The oxygen spectra, with a peak at 532.0 eV, shows that this element is only present as a surface oxide layer, with very little oxygen in the bulk of the material and that it is bonded only to silicon [22]. These results have also been confirmed from ion beam analysis. It may be noticed in Fig. 1a, b and d that after etching 100 nm only SiC is detected.

It is observed that the presence of Si–O, C–C and Si–C bonding, in the near-surface region of the coatings, has strong dependence upon the deposition conditions like plasma power, substrate temperature and methane concentration. It is important to emphasize that the increase in the percent of Si–C and the corresponding decrease in the percents of Si–O and C–C bonding suggest that at lower temperature and CH_4 concentration, more Si–C bonds are formed from the breaking of Si–O and C–C bonds. To elucidate the relationships between the different types of bonding in the samples the area of the simulated component peaks from the second sets of XPS data the ratios, Si–O/Si–C, C–C/C–Si, were calculated for the region near the surface of samples.

Fig. 2 shows the variation of Si–O/Si–C and C–C/C–Si ratios as a function of the substrate temperature. It can be seen that the variation of these proportions is very similar up to T_s=900 °C. Above T_s, the graphitic phase starts to decrease while the oxide layer in the surface layer remains almost constant.

Fig. 3a and b show the variation of the Si–O/Si–C and C–C/C–Si ratios with the percentage of CH_4 in the gas for plasma powers of 100 and 200 W. In general, the higher the concentration of CH_4 the greater the amount of oxide and amorphous carbon present in the surface. However, RF plasma plays an important role in decreasing the amorphous phase in the surface of the film. It is observed that at higher plasma power, the graphitic phase is decreased while the oxide layer is increased.

Fig. 4 shows a typical FTIR spectra of a sample prepared using a gas ratio of Ar/CH_4=70/30, a plasma power of 200 W and a temperature of 850 °C, very similar spectra were obtained for the other conditions. No appreciable evidence of either Si–H or C–H bonding is observed, in agreement with the XPS peak assignment.

If a uniform SiC film was assumed for the simulation of the data obtained by ellipsometry a good fit between the experimental and theoretical data could not be obtained. It was found that the best possible fitting was achieved by using a multi-layer model. The fitting parameters (see Eq. (2)) are: ε_∞=2.923, f_1= 55.856, ω_{01}=0.4801, γ_1=19.355, f_2=5.145, ω_{02}=5.505, γ_2=1.514. The stack, shown in Fig. 5, consisted of the Si (100) substrate, its natural oxide layer (SiO_2, 24 Å thick), a layer of SiC+ voids (2000 to 7000 Å thick), and a composite surface layer of SiO_2+SiC (60 to 130 Å thick and a concentration of SiO_2/SiC of 30% to 80%). Even though surface of films is rough, interfaces were assumed sharp, therefore, the effect of roughness is not

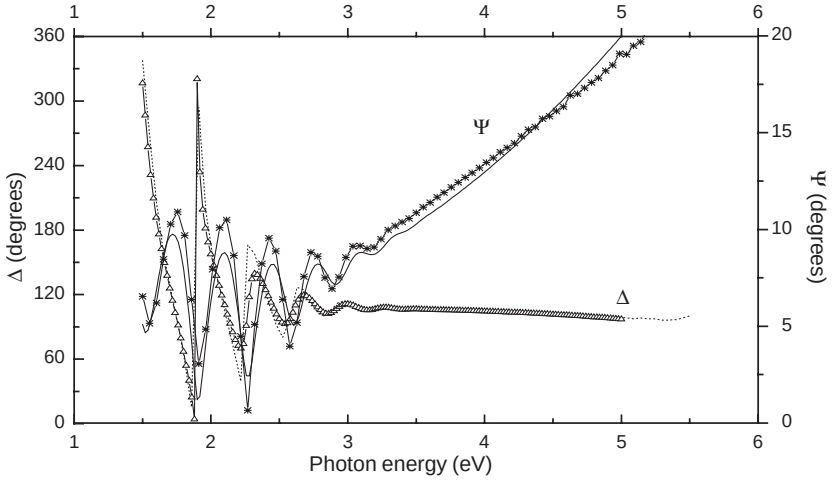

Fig. 6. The results of curve fitting of the ellipsometer experimental data (ψ, Δ) for a SiC thin film described in the text. Data are the curves traced through the symbols and the continuous lines correspond to the fitting of the data.

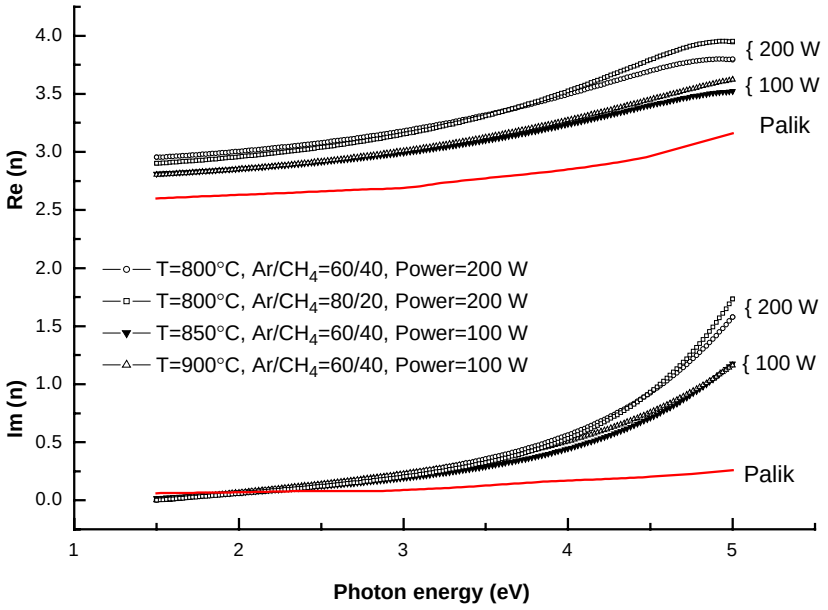

Fig. 7. A comparison of complex refractive index based on our measurements and those from Choyke and Palik.

considered. Roughness is an important factor when considering the oxidation of a surface. The volume fraction and thickness of the last layer was seen to vary from sample to sample. The equivalent refractive index of the composite layer was calculated by the effective medium approximation theory. The experimental and modelled curves were compared using a least square process by minimising $\chi^2=\sum[(\psi_m-\psi_e)^2+(\Delta_m-\Delta_e)^2]$, where the indices m and e correspond to modelled and experimental values, respectively. Fig. 6 shows an example of this process for a film prepared at RF-power of 200 W, $Ar/CH_4=70/30$ and substrate temperature of $T_s=950$ °C. In general, the agreement was very good for all films.

The Fig. 7 presents a comparison of complex refractive index based on our measurements and those from Choyke and Palik [25]. The imaginary part of the refractive index, *Im(n)*, is larger in our films and, consequently, the absorbance is also higher, particularly in the violet and UV region. The absorption coefficient, α, is calculated from the imaginary part of the refractive index [26]. $\alpha^{1/2}$ is then plotted as a function of photon energy (Tauc plot) from which the band gap may be extracted by extrapolation as

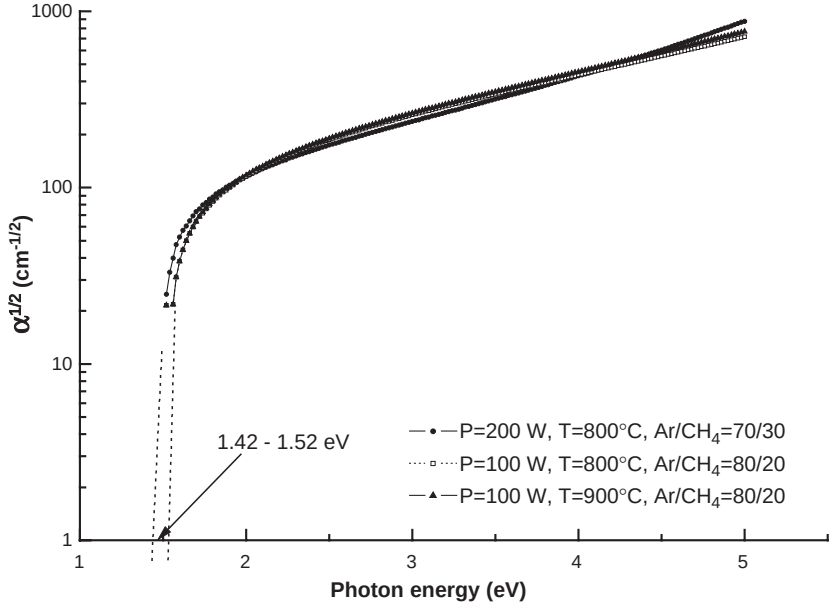

Fig. 8. Square root of the absorption coefficient, $\alpha^{1/2}$, as a function of the photon energy.

shown in Fig. 8. In this figure it may also be noticed that the band gap varies from 1.42 to 1.52 eV, depending on the deposition parameters.

4. Discussion

Deposition parameters have a strong influence on the optical and surface properties. Films prepared using different deposition conditions are separated into two groups in the refractive index vs. photon energy graphs, one corresponding to the plasma power=200 W (higher n) and the other to 100 W (lower n). This probably indicates the importance of ion bombardment during the growth of this material since for these stoichiometric films it can be assumed that the value of the refractive index is proportional to the film density, and the higher density plasma, associated plasma potential and higher applied voltage for the 200 W power case can be expected to result in a greater degree of ion bombardment of the substrate.

The XPS measurements reinforce the ellipsometer model since both techniques reveal the presence of oxygen in the external layers of the films, even though the deposits were cooled to less than 100 °C before being exposed to the atmosphere. However, the out-diffusion of Ar from the surface layer probable occurred during the cooling. During the formation of the oxide it appears that the oxygen replaces the carbon atoms originally bonded to silicon causing the accumulation of amorphous carbon in the surface. Moreover, it is observed that when higher substrate temperatures or methane gas concentrations are used, the formation of this oxide layer is enhanced. This has been corroborated by ellipsometry, where a 60 to 100 Å thick layer of composite material (SiO_2+SiC) is required to improve the curve fitting. From Fig. 3a it can be seen that the formation of the amorphous carbon is reduced at higher plasma powers, although this not so for the oxide layer, this is probably a result of the increased ion bombardment of the growing film which gives rise to a deposit with a somewhat increased density or improved morphology.

XPS peaks associated with hydrogen bonded to either carbon or silicon were not seen in any of the spectra, in agreement with the FTIR characterisation of the films. FTIR spectrum of the SiC films demonstrates that the fundamental absorption of SiC for the samples to occur at about 783 cm^{-1}. The absence of C–H and Si–H absorption peaks in the FTIR spectra demonstrates that the main bonding in our films is of SiC.

SiC has been studied by other groups by reflectometry of single crystals [25], and in the form of thin films by ellipsometry [29,30]. Although Choyke and Palik [25] showed that SiC in form of hexagonal platelets has a weak absorbance, our results on thin films show higher values than theirs which is probably due to slight differences in composition, as reported in our earlier paper, and to the different densities of our material. However, our results are very similar to those reported in Ref. [27], for thin films also measured by ellipsometry.

The band gap for our sputter amorphous SiC films at, $Eg \approx 1.4 \pm 0.1$ eV, is somewhat lower than similar hydrogenated amorphous silicon carbide thin films prepared by the RF-PECVD technique (1.64–2.1 eV) [27] but comparable to the work of Seaward et al. who prepared crystalline, β-SiC, films by dual-source sputter deposition (1.43 eV) [28]. However, it is higher to the similar films prepared by laser ablation technique (1.0 eV) [31].

The high quality native oxide layer in SiC is important for use as MOS. In our case this oxide layer is present in all deposition conditions. However, this SiO_2 layer is higher at higher substrate temperature or lower CH_4 concentration in the mixture of reactive gases in the vacuum chamber. It is observed that thermal oxidation of SiC produces a layer of SiO_2 on the surface while the carbon atoms from the SiC form CO which escapes as a gas. However, some graphitic phase C–C is still present on the surface, which can be decreased for lower concentration of CH_4 in the presence of energetic plasma (RF power=200 W) while the oxide layer is increased for higher plasma power. Thus it is observed that by using the appropriate deposition parameters, it is possible to prepare a good quality SiC thin film having a surface oxide layer, SiO_2, suitable for use as an MOS insulator with minimum concentration of graphitic phase by RF-RMS technique.

5. Conclusions

The surface and optical properties have a strong dependence on the deposition parameters. The surface of silicon carbide films prepared by reactive magnetron sputtering are seen to have compositions different from the bulk value, including the formation of a considerable oxide layer mixed with amorphous carbon, even though the temperature of the film was less than 100 °C before being exposed to atmosphere. This surface layer is enhanced when high substrate temperatures and/or high methane gas concentrations are employed in the film preparation.

The near surface of SiC exposed to atmosphere was primarily composed of SiO_2 along with amorphous carbon while the bulk of the material was SiC. At higher plasma power and lower CH_4 concentration, the graphitic phase in the surface decreases and the refractive index increases while the surface oxide layer remains present. All films prepared at different deposition conditions present a composition close to SiC stoichiometry, (even for CH_4 to Ar gas concentrations below 1:2).

Our measurements indicate that the hydrogen present in the precursor mixture is not included chemically in the deposited film under the conditions used in the present study.

Acknowledgements

Technical assistance and fruitful discussions with J.A. Díaz and F.F. Castillón are gratefully acknowledged.

References

[1] Gautam Ganguly, Subal C. De, Swarty Ray, A.K. Barua, J. Appl. Phys. 69 (7) (1991 (April)) 1.
[2] T.M. Parrill, C.W. Chung, Surf. Sci. 243 (1991) 96.
[3] G.L. Harris, C.Y.-W. Yang (Eds.), Amorphous and Silicon Carbide, Spring Proceedings in Physics, vol. 34, Springer Verlag Berlin, Heidelberg, 1989, p. 34.
[4] A. Tran, D. Fung, M.M. Rahman, C.Y.-W. Yang, in: G.L. Harris, C.Y.-W. Yang (Eds.), Amorphous and Crystalline Silicon Carbide and Related Materials, Spring Proceedings in Physics: Proceedings of the 1st International Conference, Washington DC, December 10–11, 1987, vol. 34, Springer, New York, 1987, p. 83.
[5] CRC Handbook of Chemistry and Physics, 76th ed., CRC Press, West Palm Beach, FL, 1996.
[6] H.J. Kim, R.F. Davis, J. Electrochem. Soc. 133 (1986) 2350.
[7] J. Bullet, M.P. Schmidt, Phys. Status Solidi 143 (1987) 345.
[8] Z. Chen, K. Yang, R. Zhong, H. Shi, Y. Zheng, in: D.K. Gaskill, C.D. Brandt, R.G. Nemanich (Eds.), III-Nitrides, SiC and Diamond Materials for Electronic Devices, Materials Research Society Symposium Proceedings, vol. 423, 1996, p. 753.
[9] K. Sagra, E. Murakami, Appl. Phys. Lett. 54 (1989) 2003.
[10] T. Matsuyama, T. Baba, T. Takahama, S. Tsuda, S. Nakano, Sol. Energy Mater. Sol. Cells 34 (1994) 285.
[11] S. Veprek, Mater. Res. Sol. Symp. Proc. 164 (1990) 39.
[12] T. Sugil, T. Aoyama, T. Ito, J. Electrochem. Soc. 3 (1990) 989.
[13] C.A. Dimitriadis, J. Stoemenos, P.A. Coxon, S. Friligkos, J. Antonopoulis, N.A. Economous, J. Appl. Phys. 73 (1993) 8402.
[14] S. Motoyama, H. Mitsui, Y. Tarui, T. Fuyuki, H. Matsunami, J. Appl. Phys. 68 (1990) 101.
[15] Q. Wahab, R.C. Glass, I.P. Ivnaov, J. Birch, J.E. Sundgren, M. Willander, J. Appl. Phys. 74 (1993) 1663.
[16] Q. Wahab, M.R. Sardela, J.L. Hultman, et al., Appl. Phys. Lett. 65 (1994) 725.
[17] E. Andrade, Nucl. Instrum. Methods Phys. Res., B Beam Interact. Mater. Atoms 57 (1991) 799.
[18] M. Mayer, SIMNRA User's Guide, Technical Report IPP 9y.
[19] Max-Plank-Institut fur Plasmaphysik, Garching, Germany.
[20] R. Doolittle, Nucl. Instrum. Methods Phys. Res., B Beam Interact. Mater. Atoms 15 (1986) 227.
[21] R.M. Azzam y, N.M. Bashara, Ellipsometry and Polarised Light, North-Holland, 1987.
[22] L. Ottaviani, D. Planson, M.L. Locatelli, J.P. Chante, B. Canut, S. Ramos, Mat. Sci. Forum 264–268 (1998) 709.
[23] R.C. Lee, C. Rubin Aita, N.C. Tran, J. Vac. Sci. Technol., A, Vac. Surf. Films 9 (1991) 1351.
[24] W.K. Choi, T.Y. Ong, L.S. Tan, F.C. Loh, K.L. Tan, J. Appl. Phys. 83 (1998) 4968.
[25] W.J. Choyke, E.D. Palik, in: E.D. Palik (Ed.), Handbook of Optical Constants of Solids, Academic Press, 1985.
[26] J.I. Pankove, Optical Processes in Semiconductors, Dover Pub., 1971, p. 34.
[27] E. Pascual, J.L. Andújar, J.L. Fernández, E. Bertran, Diamond Relat. Mater. 4 (1995) 702.
[28] K.L. Seaward, T.W. Barbee Jr., W.A. Tiller, J. Vac. Sci. Technol., A, Vac. Surf. Films 4 (1986) 31.
[29] Shenghong Yang, Dihu Chen, Huiqui Li, Yueli Zhang, Dang Mo, S.P. Wong, Solid State Commun. 116 (2000) 177.
[30] R. Machorro, E.C. Samano, G. Soto, L. Cota, Appl. Surf. Sci. 127 (1998) 564.
[31] R. Machorro, E.C. Samano, G. Soto and L. Cota, Private communication.